Prem Kumar Seelam*, Anne-Riikka Rautio, Mika Huuhtanen, Krisztian Kordas and Riitta L. Keiski

Low temperature steam reforming of ethanol over advanced carbon nanotube-based catalysts

DOI 10.1515/gps-2015-0014
Received February 28, 2015; accepted April 21, 2015; previously published online June 30, 2015

Abstract: Steam reforming of biofuels such as bioethanol offers a clean and sustainable route to improve hydrogen production capacity for the hydrogen economy. In this work, the influence of the carbon support type (carbon nanotube [CNT], activated carbon [AC] and graphitic carbon black [GCB]) and the addition of Pt (1 wt.%, 1.5 wt.% and 2 wt.%) and ZnO (10 wt.%) to Ni_{10}/CNT (10 wt.% Ni) are studied in steam reforming of ethanol (SRE) at low temperatures (≤450°C). The prepared CNT-based catalysts were characterized by nitrogen physisorption, X-ray powder diffraction (XRD), energy-dispersive X-ray (EDX) and energy filtered transmission electron microscopy (EFTEM) analyses. Ni supported on CNTs was found to be highly active for SRE compared to other conventional carbon supported catalysts. The promotional effect of Pt in the $Ni_{10}Pt_x$/CNT catalysts was found to be unexpectedly insignificant in terms of ethanol conversion, hydrogen production and selectivity. By contrast, the hybrid $(ZnO)_{10}Ni_{10}$/CNT catalyst showed superior catalytic performance below 450°C with high H_2 selectivity and low CO selectivity compared to all other CNT-based catalysts. The Ni_{10}/CNT catalyst undergoes rapid deactivation compared to the ZnO promoted Ni_{10}/CNT due to the large amounts of carbon deposition on the catalyst. The ZnO promoted Ni_{10}/CNT catalyst enhances the hydrogen production and reduces the carbon formation, making the catalyst attractive for the SRE reaction.

Keywords: CNT; hydrogen production; Ni; ZnO.

***Corresponding author: Prem Kumar Seelam,** Environmental and Chemical Engineering Research Group, Faculty of Technology, P.O. Box 4300, University of Oulu, Finland, e-mail: prem.seelam@oulu.fi
Anne-Riikka Rautio and Krisztian Kordas: Microelectronics and Materials Physics Laboratories, Department of Electrical Engineering, P.O. Box 4500, University of Oulu, Finland
Mika Huuhtanen and Riitta L. Keiski: Environmental and Chemical Engineering Research Group, Faculty of Technology, P.O. Box 4300, University of Oulu, Finland

1 Introduction

Nowadays, most hydrogen is produced by catalytic steam reforming of natural gas over nickel catalysts [1]. The demand for hydrogen supply is continuously increasing due to the renewable energy needs and the increased use of hydrogen in process industries [2]. Since it is of outmost importance to produce energy in an efficient, sustainable and environmentally friendly way, bio-derived alcohols are very attractive options as sources of hydrogen and are expected at least partly to replace fossil hydrocarbons in the future fuel economy [3–5].

Steam reforming of ethanol [SRE, Eq. (1)] is a widely studied reaction at temperatures above 550°C by applying a number of different catalytic materials. The most active catalysts are found to be Rh, Pt and Pd [6, 7] supported on Al_2O_3, ZrO_2, CeO_2, zeolites and SiO_2 [8], however, Ni-, Co- and Ru-based catalysts also hold promise as affordable choices for efficient and selective catalysts. Production of hydrogen at low temperatures is very challenging. Interestingly, oxygenates including alcohols can be reformed at lower temperatures [9, 10] than hydrocarbons such as methane and propane [11, 12]. Thermodynamically, the dominant product compounds in SRE include H_2, CH_4, CO, CO_2, CH_3CHO, C_2H_4 and carbon [13, 14]. At temperatures below 400°C, ethylene and acetaldehyde are the main intermediates [Eqs. (2) and (3)]. The main routes for carbon formation are via ethylene polymerization [Eq. (4)] and CO disproportionation reactions [Eq. (11)] causing potential catalyst poisoning [6, 8, 9]. The type of carbon formed (soot, fibers and nanotubes) depends on the operating conditions and on the catalyst as well.

The following important parallel reactions (1–12) occur during the SRE [8, 13, 15]:

$$\text{Overall SRE: } C_2H_5OH + 3H_2O \rightleftharpoons CO_2 + 6H_2 \quad (1)$$

$$\text{Dehydrogenation of ethanol: } C_2H_5OH \rightleftharpoons CH_3CHO + H_2 \quad (2)$$

$$\text{Ethanol dehydration: } C_2H_5OH \rightleftharpoons C_2H_4 + H_2O \quad (3)$$

$$\text{Ethylene polymerization: } C_2H_4 \rightarrow \text{polymer} \rightarrow \text{carbon} \quad (4)$$

$$\text{Ethanol decomposition: } C_2H_5OH \rightarrow CH_4 + CO + H_2 \quad (5)$$

$$\text{Acetaldehyde decomposition: } CH_3CHO \rightarrow CH_4 + CO \quad (6)$$

$$\text{Acetaldehyde reforming: } CH_3CHO + 3H_2O \rightleftharpoons 2CO_2 + 5H_2 \quad (7)$$

$$\text{CO methanation: } CO + 3H_2 \rightleftharpoons CH_4 + H_2O \quad (8)$$

$$\text{Carbon gasification: } CO + H_2 \rightleftharpoons H_2O + C \quad (9)$$

$$\text{Water-gas-shift: } CO + H_2O \rightleftharpoons CO_2 + H_2 \quad (10)$$

$$\text{Boudouard reaction: } 2CO \rightleftharpoons CO_2 + C \quad (11)$$

$$\text{Methane decomposition: } CH_4 \rightarrow 2H_2 + C \quad (12)$$

For proton exchange membrane type fuel cells, in which the catalytic electrodes are based on Pt catalysts, the reformate stream should have very low concentration of CO (below 10 ppm) and other compounds than H_2 [16] in order to avoid poisoning of the anode catalyst. To produce CO-free reformate, additional purification steps such as the water-gas-shift, CO oxidation or membrane purification are needed. Therefore, it is important to reduce the CO and CH_4 concentration to minimize or eliminate operating costs of the downstream purification steps. However, the concentration of CH_4 is typically very low at temperatures below 400°C. By contrast, at temperatures higher than 550°C, the rapid formation of CO is a serious concern and has been proposed to be minimized by using low temperature SRE processes [14, 17, 18].

In the catalytic steam reforming, not only the metal, but also the nature of catalyst support plays an important role at low reaction temperatures by influencing the product distribution [19, 20]. The Ni/ZnO catalyst is known to outperform pure Ni in SRE [21] due to the good water activation properties of ZnO [22–24]. The robustness and reasonably high specific surface area along with the accessible pore structure in a multiwalled carbon nanotube (CNT) make it an ideal candidate for a catalyst support in moderate conditions [25–28]. Studies on steam reforming of bio-oil [29], methanol [30], propane [31] and ethanol [10, 32] over CNT supported catalyst nanoparticles have been reported. In López et al. [31], a Ni/multiwalled CNT catalyst was tested in a propane steam reforming reaction. Due to controlled Ni dispersion over CNTs, the optimal metal content and particle size facilitated higher activity and H_2 selectivity compared to a commercial Ni/Al_2O_3 catalyst. It has been noted that adding metals and oxides as co-catalysts improves the overall catalytic properties of Ni [33–40]. Small amounts of Pt, Cu, or ZnO added into Ni catalysts can enhance the activity and reduce the coke formation [18, 20, 33, 36]. The promoters have a strong influence on the reducibility and dispersion of the metal catalysts [22, 24, 39–42]. Therefore, the primary goal of this work was to find out whether the addition of a secondary metal (Pt) and a metal oxide (ZnO) to a Ni catalyst on a CNT support could improve the overall catalytic performance of the catalyst.

2 Materials and methods

2.1 Catalyst preparation

Multiwalled CNTs (Sigma-Aldrich, inner diameter×outer diameter×length=2–6 nm×10–15 nm×0.1–10 μm, USA) were pretreated in nitric acid in order to remove amorphous carbon and to introduce polar groups on the structure [43]. The pretreatment was done in the following way: CNTs were sonicated and refluxed in 70% HNO_3 (70%, Sigma-Aldrich, ACS reagent, Germany) for 3 h and 8 h, respectively, followed by rinsing, centrifuging and decanting several times with deionized water, and drying. The nickel ($Ni(acac)_2$, 95%, Aldrich, USA) decorated CNT samples were prepared by a wet impregnation method with 10 wt.% Ni nominal loading as described elsewhere [10]. Reduction was made under 15% H_2/Ar flow at 250°C for 15 min. Preparation of Pt promoted $Ni_{10}Pt_x$/CNTs (10 wt.% Ni and x=1 wt.%, 1.5 wt.% and 2 wt.% Pt) were done by mixing the reduced Ni_{10}/CNT catalyst with 40 cm^3 of ethanol (99.5%, Altia, Finland) and the required amount of $Pt(acac)_2$ (99.99%, Aldrich, USA) solution in 200 cm^3 of water. The ZnO promoted Ni/CNTs were also prepared with 10 wt.% ZnO (Zinc acetate, 99.99%, Aldrich, USA) in the same procedure by using basic water solution. All other carbon supported catalysts, i.e. activated carbon [AC (FLUKA, purum, Belgium)] and graphitic carbon black (GCB, <20 μm, Aldrich, Switzerland) were pretreated and synthesized in a similar procedure as the CNT-based catalysts with 2 wt.% Ni loadings. Commercial 16.6 wt.% Ni/Al_2O_3 catalyst pellets (HTC400, Crosfield, Warrington, England) crushed and sieved to a powder form (<250 μm particle size) was used as a reference catalyst.

2.2 Catalyst characterization

The specific surface area (S_{BET}), pore size and pore volume were analyzed by N_2 adsorption-desorption isotherms at -196°C using Micromeritics ASAP2020, USA. The surface area of catalyst samples and the pore size/volume were calculated by the Brunauer-Emmett-Teller (BET) and Barrett-Joyner-Halenda methods, respectively.

Catalyst materials were characterized with X-ray powder diffraction (XRD, Siemens D5000, USA, CuK_α –radiation) to determine the phase and volume averaged crystal size of the catalyst particles (from the fitting parameters of Lorentzian functions over the reflected intensity peaks). The metal content of the samples was measured by energy-dispersive X-ray analysis (EDX, Inca installed on Zeiss Ultra plus FESEM, Germany). Elemental concentrations were measured from at least three locations of each specimen. The average particle size and particle size distribution were determined from energy filtered transmission electron microscopy (EFTEM, LEO 912 OMEGA, Germany, acceleration voltage 120 kV) images by measuring at least 100 particles from each sample.

2.3 Catalyst activity test

In the activity experiment, 100 mg of a metal decorated CNT-based catalyst was packed with quartz wool in a tubular quartz reactor with an inner diameter of 8 mm. The catalyst sample was pretreated and reduced in 20% H_2 (in N_2) with 80 cm^3 min^{-1} flow rate by heating from room temperature up to 350°C with a rate of 15°C min^{-1} followed by reduction at 350°C for 30 min, and cooled down to room temperature under the same gas flow. The SRE reaction was tested from 150°C to 450°C with a heating rate of 10°C min^{-1}. The liquid ethanol-water mixture (molar ratio of 1:3) of 0.091 cm^3 min^{-1} was fed into the reactor by a peristaltic pump with a total flow rate of 600 cm^3 min^{-1} (N_2 as carrier gas). All of the experiments were carried out under atmospheric pressure with a constant gas hourly space velocity (38,000 h^{-1}). The catalyst activity was evaluated based on the outlet concentrations measured by a Fourier transform infrared (FTIR) spectrometer (GASMET) and XMTC H_2 analyzer. The performance of the tested catalysts in SRE was evaluated in terms of ethanol conversion, hydrogen production rate, product compositions and hydrogen selectivity.

3 Results and discussion

3.1 Structural properties

The surface characteristics i.e. surface area (S_{BET}), pore size and pore volume of the Ni-based CNT catalysts and also the reference catalyst (Ni/Al_2O_3) are presented in Table 1. The S_{BET} values of 209–269 m^2 g^{-1} for Ni supported CNT-based catalysts are considerably higher than that of the pristine CNTs (75 m^2 g^{-1}), indicating a structural change of the support during the catalyst synthesis procedure.

During the purification and carboxylation steps, structural changes, e.g. creation of defects and scavenging of impurities, might probably have occurred on CNTs. This can result in an increase in the surface area from 75 m^2 g^{-1} to 218 m^2 g^{-1} and the pore volume from 0.22 cm^3 g^{-1} to 0.67 cm^3 g^{-1} for MWCNTs and CNT-COOH (carboxylated CNTs), respectively. Moreover, after the acidic pretreatment steps, the tip openings of tubes also contribute to the change of the overall pore structure [26, 37].

The surface area of the functionalized CNT support increased from 218 m^2 g^{-1} to 269 m^2 g^{-1} after the incorporation of Ni. The pore sizes of CNT-based catalysts varied between 9 nm and 12 nm, i.e. the samples resemble mesoporous materials. There are significant changes in the pore volume and surface area values after the pretreatment steps. By contrast, the pore volume changed dramatically for the carboxylated and Ni decorated CNTs in comparison with the pristine sample. In the textural properties of the $Ni_{10}Pt_x$/CNT catalysts, no differences were found among the samples. There is a slight decrease in surface area in NiPt-based catalysts due to Pt dispersed on the exterior surface of the tubes. However, in the case of ZnO promoted catalysts, i.e. $(ZnO)_{10}Ni_{10}$/CNT, the surface area is decreased from 269 m^2 g^{-1} to 209 m^2 g^{-1} due to bigger ZnO particles dispersed on the tube surface, which also blocks the tube openings. For $Ni_{10}(ZnO)_{10}$ and $(ZnO)_{10}Ni_{10}$/CNT-based catalysts, a bigger difference appears in the S_{BET} and pore characteristics compared to Ni_{10}/CNT, due to the presence of relatively large ZnO particles in the samples. The reference catalyst Ni/Al_2O_3 exhibits lower S_{BET} and pore volume values compared to the Ni-decorated CNT-based catalysts.

The TEM analyses of the Ni_{10} and $Ni_{10}Pt_x$ (x=1–2 wt.%) CNT-based catalysts (Figure 1) show that the average Ni nanoparticle size varies from 3.5 nm to 4.8 nm for all $Ni_{10}Pt_x$/CNT catalysts. As reported by Halonen et al. [26], due to the tube confinement effects in CNTs, small particles with a narrow size distribution are obtained. It is difficult to distinguish between the Ni and Pt nanoparticles (Figure 1) as the Ni loading (10 wt.%) is much higher than that of Pt (1–2 wt.%). Some of the nanoparticles might be present in the interior of the nanotubes [27]. Since the inner diameter of the nanotubes is around 2–6 nm and the kinetic diameter of the reactant and product molecules is less than 2 nm [38], the reaction might also occur in the inner cavity of the nanotubes [38]. In the $Ni_{10}Pt_x$/CNT (x=1–2 wt.%) catalysts, the Pt(111) metallic phase was observed at $2\theta=40^o$ (Figure 1). The peak intensity of the NiO phase might have been reduced because of the formation of new crystal planes in the $Ni_{10}Pt_x$/CNT and that might have enhanced the reducibility of Ni^{2+} to Ni^0 for promoted catalysts. This phenomenon has been reported over various NiPt catalysts, e.g. in [35, 36, 42, 45] and thus, it is expected that Ni will be reduced more easily on CNT when Pt and ZnO are present [41, 42, 45].

Table 1: Textural properties of fresh carbon nanotube (CNT)-supported catalysts results are adapted from [44], copyrights permission form University of Oulu.

Catalyst	BET (m^2 g^{-1})	Pore volume (cm^3 g^{-1})	Pore size (nm)
MWCNT-pristine[a]	75	0.22	11.4
CNT-COOH	218	0.67	11.9
Ni_{10}CNT	269	0.66	9.4
$Ni_{10}Pt_1$CNT	258	0.72	10.9
$Ni_{10}Pt_{1.5}$CNT	251	0.70	10.8
$Ni_{10}Pt_2$CNT	251	0.75	11.6
$(ZnO)_{10}Ni_{10}$CNT	209	0.56	10.4
$Ni_{10}(ZnO)_{10}$CNT	241	0.63	10.1
$Ni_{16.6}/Al_2O_3$[b]	112	0.33	11.8

[a]Untreated CNTs.[b]Reference catalyst. BET, Brunauer-Emmett-Teller; MWCNT, multiwalled carbon nanotube.

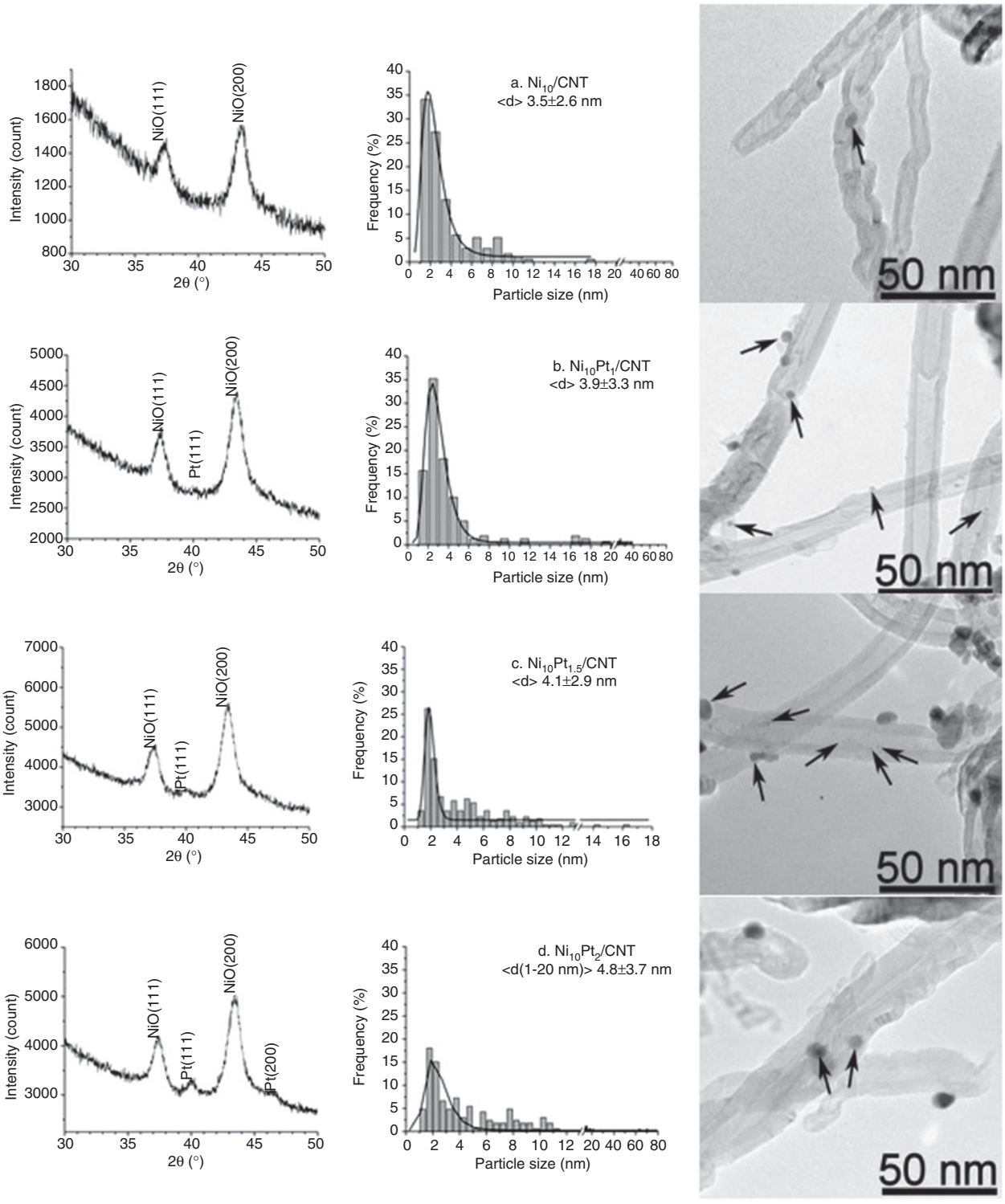

Figure 1: X-ray powder diffraction (XRD) patterns and energy filtered transmission electron microscopy (EFTEM) images of (A) Ni_{10}/carbon nanotube (CNT), (B) $Ni_{10}Pt_1$/CNT, (C) $Ni_{10}Pt_{1.5}$/CNT and (D) $Ni_{10}Pt_2$/CNT catalysts.

Before the reduction step, X-ray diffraction analyses indicate that the oxide phases, i.e. NiO and ZnO, were present (Figure 2). The bigger particles observed in the TEM images were assigned as ZnO according to the very narrow reflection peaks in the corresponding X-ray diffraction patterns. For $Ni_{10}Pt_x$/CNT catalysts, no reflections were detected from the alloy, thus indicating that no alloy was formed.

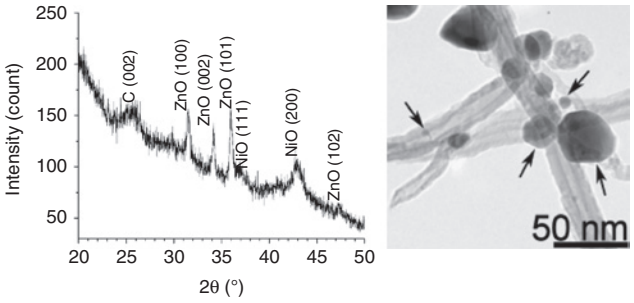

Figure 2: X-ray powder diffraction (XRD) pattern and energy filtered transmission electron microscopy (EFTEM) micrograph of $(ZnO)_{10}Ni_{10}$/carbon nanotube (CNT) catalyst.

From the EDX analyses, small amounts of Al and Fe impurities are detected, indicating that the catalyst used for growing the CNTs was not completely removed during the support preparation. The elemental composition of fresh and used CNT-based catalysts was analyzed by EDX and summarized in Table 2. The Ni and Pt contents (wt.%) in the NiPt-based catalysts were higher than the nominal loadings due to the partial oxidation of the carbon content.

As the amount of added Pt increased (from 1 wt.% to 2 wt.%), the heterogeneity of the sample increased due to its non-uniform distribution of Pt (Table 3). The average crystal size measured by XRD (using the Scherrer equation) was found to have larger values compared to those received from the TEM analysis.

3.2 Influence of carbon support type

Three different carbon-type supports with 2 wt.% Ni as the nominal loading were prepared and denoted as Ni_2/CNT, Ni_2/GCB and Ni_2/AC catalysts. The nature of the carbon support (AC and GCB) was studied in SRE and the samples were prepared with a similar procedure and the same Ni metal content as CNTs. Based on TEM, the Ni nanoparticles are finely dispersed and decorated over the surface of the CNTs compared to other carbon supports (figures not presented). The average particle size for Ni_2/CNT was 2 nm which was lower than that for Ni_2/GCB (3.3 nm) and Ni_2/AC (4.9 nm). Over the Ni_2/CNT catalyst, it was found that a more narrow distribution of particle sizes was achieved than on other carbon supports [44].

As presented in Figure 3A and B, the ethanol conversion and hydrogen production rate is higher for Ni_2/CNT in comparison with the other carbon supported Ni-based catalysts. The results correlated with the highly dispersed Ni particles, size and the narrow distribution on the support [31]. The Ni_2/CNT catalyst exhibits the highest activity and selectivity in the SRE reaction due to tube confinement effects of the CNTs. The results are in good agreement with the previous studies on CNTs [29, 31].

3.3 Influence of Pt addition on Ni/CNT

Overall, the $Ni_{10}Pt_x$-based catalysts resulted in a slight improvement in the ethanol conversion (above 300°C) and hydrogen production (around 300–400°C) was seen compared to the reference catalyst (Figure 4A and B). The Ni particle size increased slightly after the Pt addition and had a positive influence on the SRE activity. There might be two main effects induced by adding Pt, i.e. first, the Ni nanoparticles size increased due to successive thermal treatments, and second, the reducibility of NiO particles probably increased at low temperatures, thus forming

Table 2: The metal content by energy dispersive X-ray spectroscopy (EDX) analysis of fresh and used carbon nanotube (CNT)-supported catalysts.

Catalyst	Elemental concentrations (wt.%)				
	C	O	Ni	Pt	Zn
CNT-COOH	91.8±3.8	5.0±3.1	–	–	–
Ni_{10}/CNT fresh	79.9±8.4	7.5±2.6	10.7±9.3	–	–
Ni_{10}/CNT used	86.7±7.8	5.4±1.4	6.1±5.1	–	–
Pt_1Ni_{10}/CNT fresh	77.7±3.6	6.1±1.2	12.6±4.0	1.4±0.2	–
$Pt_{1.5}Ni_{10}$/CNT fresh	77.6±5.1	7.5±3.1	10.9±5.1	2.2±1.3	–
Pt_2Ni_{10}/CNT fresh	63.6±12.1	5.3±2.0	22.9±10.7	4.6±2.9	–
$(ZnO)_{10}Ni_{10}$/CNT fresh	65.4±11.8	20.4±10.6	6.9±1.9	–	5.1±3.2
$(ZnO)_{10}Ni_{10}$/CNT used	83.4±3.5	5.2±2.1	4.9±1.2	–	5.6±3.7
Ni_{10}/CNT fresh[a]	72.8±1.9	11.2±2.5	13.7±3.0	–	–
Ni_{10}/CNT used[a]	87.7±4.0	4.9±1.4	6.4±4.7	–	–

[a]Different catalyst synthesis batches.

Table 3: The average metal particle sizes of carbon nanotube (CNT)-based catalysts by X-ray powder diffraction (XRD) and transmission electron microscopy (TEM).

Catalyst	d_{TEM} (nm)	d_{XRD} (nm)
Ni_{10}/CNT	3.5±2.6	NiO(200) 5.9±0.1
Pt_1Ni_{10}/CNT	3.9±3.3	NiO(200) 5.2±0.2
$Pt_{1.5}Ni_{10}$/CNT	4.1±2.9	NiO(200) 6.3±0.1; Pt(111) 6.5±0.7
Pt_2Ni_{10}/CNT	4.8±3.7	NiO(200) 7.1±0.1; Pt(111) 10.5±0.8
$(ZnO)_{10}Ni_{10}$/CNT	n.d.	NiO(200) 6.4±0.3; ZnO(101) 28.2±1.6

n.d. not determined.

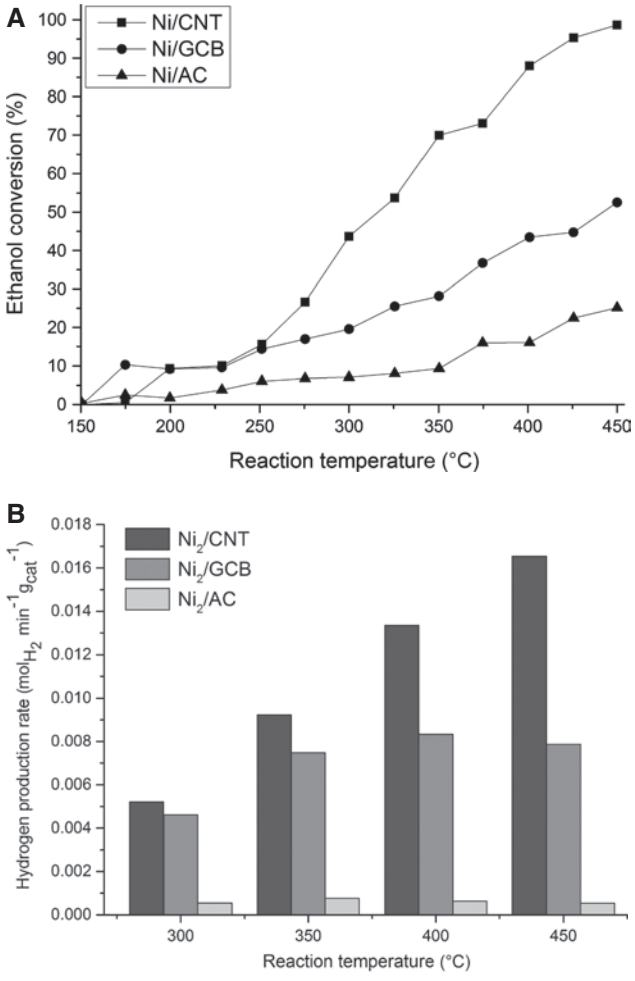

Figure 3: Nature of the type of carbon supported Ni-catalyst (Ni/carbon nanotube [CNT], Ni/graphitic carbon black [GCB], and Ni/activated carbon [AC]) in steam reforming of ethanol (SRE) on (A) ethanol conversion and (B) hydrogen production rate (in terms of mol_{H_2} min^{-1} g_{cat}^{-1}) as a function of reaction temperature.

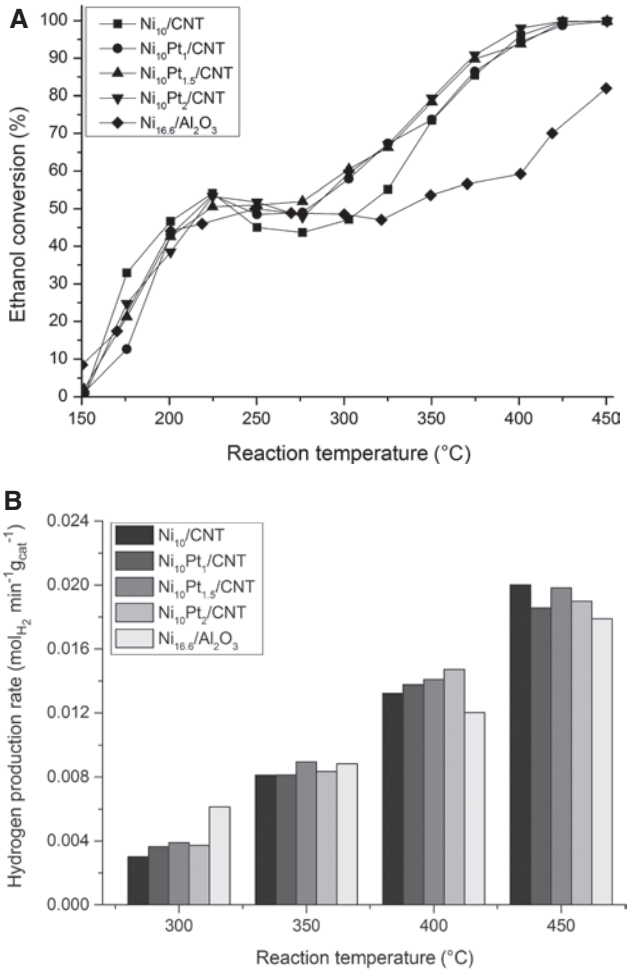

Figure 4: The effect of Pt addition on (A) ethanol conversion and (b) hydrogen production rate (in terms of mol_{H_2} min^{-1} g_{cat}^{-1}) as a function of reaction temperature for $Ni_{10}Pt_x$/carbon nanotube (CNT) (x=0 wt.%, 1 wt.%, 1.5 wt.% and 2 wt.%) and the reference catalysts in steam reforming of ethanol (SRE).

more active Ni^0 nanoparticles [36, 42, 45, 46]. Furthermore, the Pt promotion of the Ni catalyst probably prevented the oxidation of Ni with steam [35, 36]. The ethanol conversion and hydrogen production increased with temperature for all the tested catalysts. The reaction temperature had a significant effect on the reforming activity. At low temperatures, i.e. 150–275°C, the ethanol conversion in the case of the Pt promoted Ni/CNT-based catalysts was comparable to that of the commercial catalyst. Between 225°C and 300°C, ethanol conversion and H_2 production remained quite constant. It is probable that in the temperature range of 150–225°C, adsorption of ethanol is occurring and above that up to ~300°C slight desorption results in a flat plateau. Over the $Ni_{16.6}/Al_2O_3$ reference catalyst, the H_2 production is slightly higher at temperatures below 325°C, most probably due to high ethanol conversion and strong acidity character. However, the H_2 production rate per gram of catalyst values for Ni_{10} and $Ni_{10}Pt_x$ on CNT-based catalysts are higher compared to $Ni_{16.6}/Al_2O_3$ catalysts between 350°C and 450°C.

At 350°C, the maximum ethanol conversion decreased as follows: $Ni_{10}Pt_2/CNT=Ni_{10}Pt_{1.5}/CNT>Ni_{10}Pt_1/CNT=Ni_{10}/CNT>>Ni_{16.6}/Al_2O_3$ (Figure 4A). Al_2O_3 is known to be a highly acidic support, and decomposition reactions that were occurring produced intermediates such as methane and other hydrocarbons which are coke precursors, as reported in [8]. In the range from 150°C to 325°C, over the $Ni_{16.6}/Al_2O_3$ catalyst, H_2 production was more or less similar to that of the CNT-based catalysts. Above 350°C, a significantly higher hydrogen production rate was achieved over CNT-based catalysts than $Ni_{16.6}/Al_2O_3$ (Figure 4B). Over the CNT-based catalysts, a considerable amount of CH_3CHO was formed up to 400°C. In the case of the CNT-based catalysts, dehydrogenation of ethanol [Eq. (2)] was the first step to take place at 150–300°C followed by subsequent CH_3CHO reforming and disproportionation [Eqs. (6) and (10)–(12)]. The decreasing order of CH_3CHO concentration at 350°C was detected to be as follows: $Ni_{10}/CNT>Ni_{10}Pt_1/CNT>Ni_{10}Pt_{1.5}/CNT=Ni_{10}Pt_2/CNT>Ni_{16.6}/Al_2O_3$ (Figure 5A).

Over the $Ni_{16.6}/Al_2O_3$ reference catalyst, the formation of CH_3CHO was found to be very low compared to the Ni_{10}/CNT and $Ni_{10}Pt_x/CNT$ (x=1–2 wt.%) catalysts between 150°C and 400°C. At temperatures above 400°C, complete decomposition and reforming of acetaldehyde was detected over the CNT-based catalysts. The formation of CO and CH_4 was very high over the $Ni_{16.6}/Al_2O_3$ catalyst, thus decomposition of acetaldehyde might be the dominant reaction compared to reforming at low temperatures [8]. Over the CNT-based catalysts, the formation of methane showed a more or less similar trend for all the catalysts (Figure 5B). Henceforth, at low temperatures, it is difficult to control methane formation; only at high temperatures (i.e.>600°C), methane can be converted completely to H_2 and carbon oxides [11, 15]. Over $Ni_{16.6}/Al_2O_3$, the methane

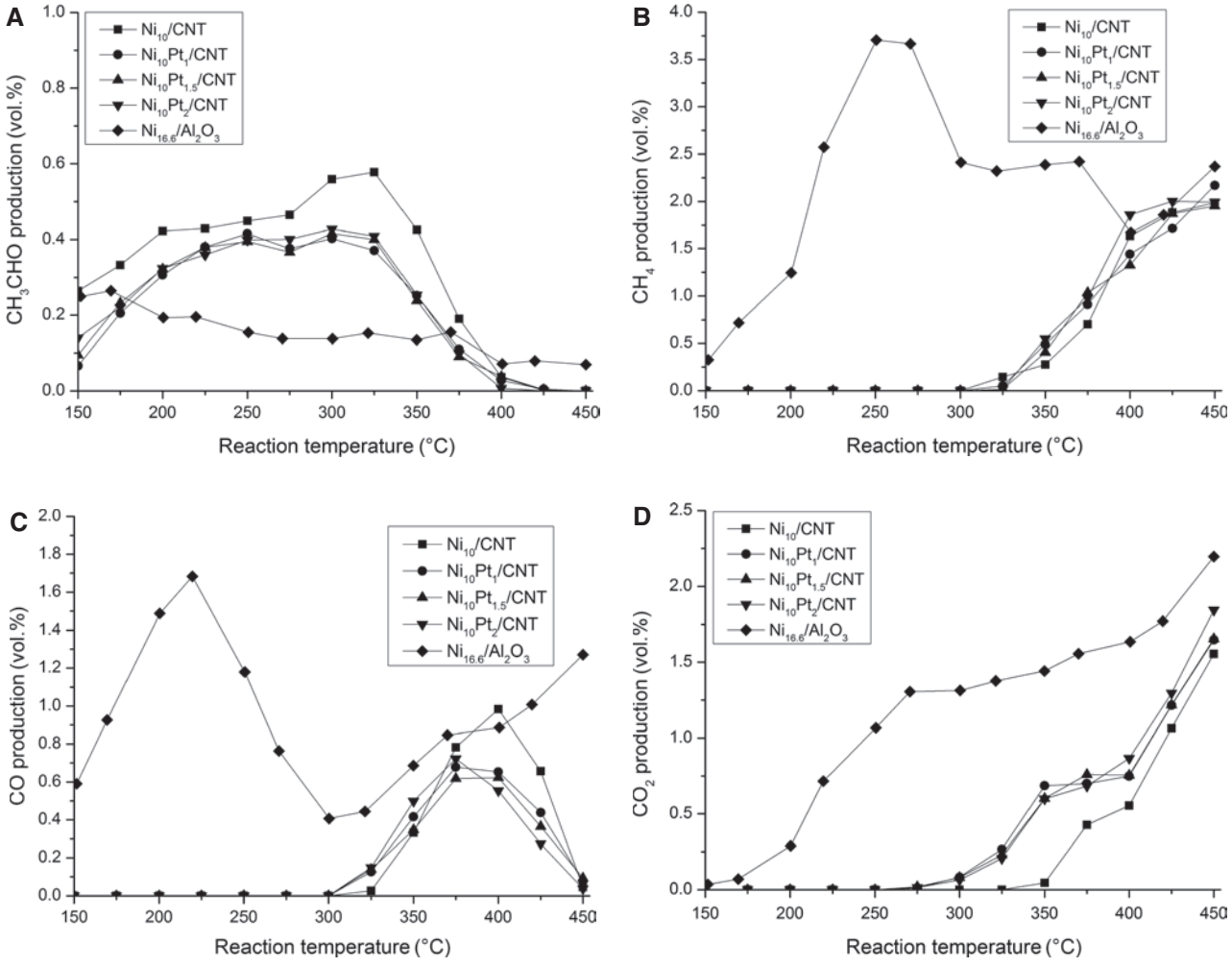

Figure 5: The concentration of products (A) CH_3CHO, (B) CH_4, (C) CO and (D) CO_2 as a function of reaction temperature over $Ni_{10}Pt_x$/carbon nanotube (CNT) (x=0 wt.%, 1 wt.%, 1.5 wt.% and 2 wt.%) and the reference catalyst in steam reforming of ethanol (SRE).

production was very high at 150–400°C compared to the CNT-based catalysts. It is also worth mentioning that the formation of ethylene was found to be high over the $Ni_{16.6}/Al_2O_3$ (figures not shown), whereas over the CNT-based catalysts, the amount of ethylene was relatively lower than 0.2 vol.%. The hydrocarbons formation detected over the Ni on alumina-based catalyst is due to the dehydration and decomposition reactions [8].

In Figure 5C and D, it can be seen that over the $Ni_{10}Pt_x$/CNT catalysts, the formation of CO and CO_2 increased at temperatures above 300°C. The CO formation increased up to 400°C, having the maxima at around 375°C, and then decreased as presented in Figure 5C. Above 400°C, the concentration of CO was detected to decline, which might be explained by two reactions; firstly, due to the water-gas-shift (WGS) reaction [Eq. (10)], and secondly, the carbon formation reactions [Eqs. (9) and (11)]. The decomposition reactions are highly pronounced over the $Ni_{16.6}/Al_2O_3$, whereas the dehydrogenation, reforming and disproportionation reactions are the possible reaction network over the CNT-based catalysts. The promotional effect of Pt was found to be slightly beneficial in CO and CH_4 reduction; a similar phenomenon was reported in [39]. Over the $Ni_{10}Pt_2$/CNT catalyst, the formation of CO_2 is observed to be the highest at 400°C compared to other $Ni_{10}Pt_x$/CNT catalysts, which can be justified by the decreasing trend in the CO concentration via WGS reaction [Eq. (10)]. Furthermore, over the $Ni_{16.6}/Al_2O_3$, CO_2 was probably formed via the Boudouard reaction [Eq. (11)], and started to increase with temperature. In the case of CNT-based catalysts, CO_2 increased with temperature due to reforming and the WGS reactions. The addition of noble metals such as Pt to Ni/CNT can probably improve the reducibility, and particle agglomeration is thus avoided as reported in some studies [34–36, 39]. Both the $Ni_{10}Pt_1$/CNT and $Ni_{10}Pt_{1.5}$/CNT catalysts behave similarly and exhibit similar values in the product composition and ethanol conversion. Overall, no significant improvement was observed in the catalytic activity after adding Pt to the Ni/CNT catalyst.

3.4 Influence of ZnO addition to Ni/CNT

ZnO was added into the Ni/CNT catalysts in two ways, i.e. ZnO was incorporated either after the Ni precursor impregnation or before the impregnation step. It can be seen from the textural properties that both the catalysts exhibit different surface characteristics. In the case of the $(ZnO)_{10}Ni_{10}$/CNT catalyst, the S_{BET} value is lower than that of the $Ni_{10}(ZnO)_{10}$/CNT catalyst (Table 1). ZnO addition modifies the surface structure of the Ni/CNT catalyst [41]. In Figure 6A, the ethanol conversion over $Ni_{10}(ZnO)_{10}$/CNT is high compared to $(ZnO)_{10}Ni_{10}$/CNT in the studied temperature range. Already, ~50% ethanol conversion was achieved over $Ni_{10}(ZnO)_{10}$/CNT at 225°C (T_{50}=225°C), and over $(ZnO)_{10}Ni_{10}$/CNT at 300°C. A complete ethanol conversion was achieved over $Ni_{10}(ZnO)_{10}$/CNT at 350°C and for $(ZnO)_{10}Ni_{10}$/CNT at 425°C. Over the $Ni_{10}(ZnO)_{10}$/CNT catalyst, the Ni particles are dispersed on the bigger ZnO particles, which indicates that more ethanol is consumed due to the proximity of Ni/NiO and ZnO particles on CNTs. Both the ZnO promoted catalysts achieved higher H_2 production (Figure 6B) than the other catalysts, i.e. Ni and NiPt-based catalysts. For both the NiZnO-based catalysts, the hydrogen production steadily increased with temperature. The $Ni_{10}(ZnO)_{10}$/CNT catalyst produced slightly higher amounts of H_2 between 150°C and 350°C

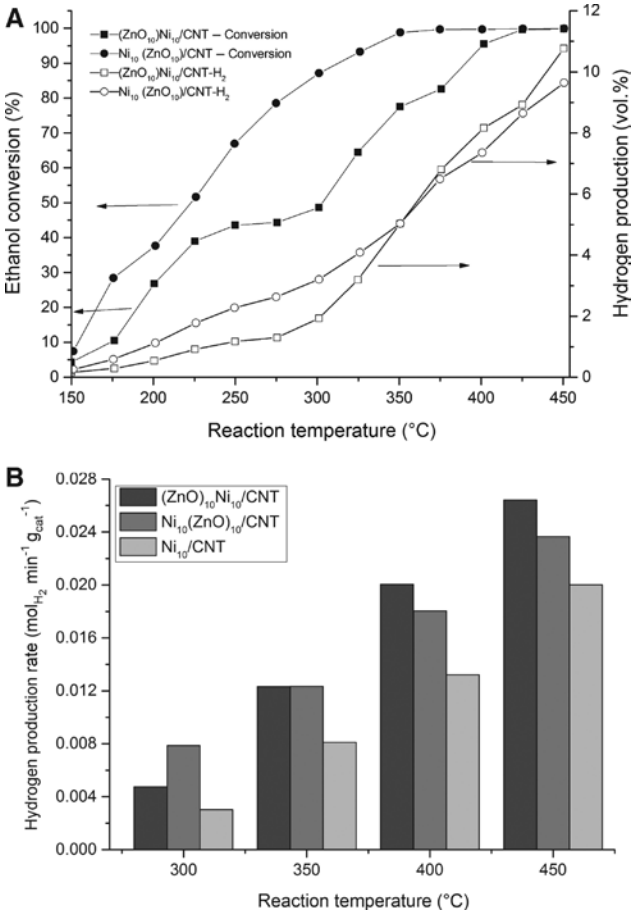

Figure 6: The effect and the mode of ZnO addition on the Ni_{10}/carbon nanotube (CNT) catalyst in steam reforming of ethanol (SRE): (A) ethanol conversion and hydrogen production as a function of the reaction temperature and (B) hydrogen production rate (in terms of mol_{H_2} min^{-1} g_{cat}^{-1}) over the ZnO promoted Ni_{10}/CNT catalysts.

compared to $(ZnO)_{10}Ni_{10}$/CNT due to the enhanced steam reforming activity and also higher conversions. At 450°C, $(ZnO)_{10}Ni_{10}$/CNT produced much higher hydrogen production rate values compared to $Ni_{10}(ZnO)_{10}$/CNT and Ni_{10}/CNT catalysts. Over the $(ZnO)_{10}Ni_{10}$/CNT catalyst we obtained the highest H_2 yield of 3.3 H_2 moles per mole of ethanol reacted compared to all other catalysts. Thermodynamic calculations made (using HSC Chemistry 7) on ethanol conversion and H_2 yield in the studied temperature range are presented in Supplemental Table 1.

By adding ZnO to the Ni_{10}/CNT catalyst, a significant improvement in catalyst activity was observed. Over the $(ZnO)_{10}Ni_{10}$/CNT catalyst, the undesirable byproducts formation was significantly lower than over the $Ni_{10}(ZnO)_{10}$/CNT catalyst (Figure 7). The concentration of CH_3CHO was relatively higher over ZnO promoted catalysts (Figure 7A) and this indicates the ethanol dehydrogenation is more pronounced than the other CNT-based catalysts. Methane is formed above 350°C, and its formation starts to increase as a function of temperature, as shown in Figure 7B. The methane formation presents a similar trend for all of the CNT-based catalysts except for the reference catalyst. Over the $(ZnO)_{10}Ni_{10}$/CNT catalyst, the CO concentration is very low in the temperature region between 200°C and 350°C (Figure 7C). For $Ni_{10}(ZnO)_{10}$/CNT, the CO concentration increases until the temperature reaches 400°C and decreases then to <0.1 vol.%. Both CO and CH_4 free regions are achieved over the $(ZnO)_{10}Ni_{10}$/CNT catalyst at temperatures below 350°C.

ZnO on the Ni_{10}/CNT catalyst probably forms bigger clusters/clumps around the Ni particles, which may enhance the oxidation of CO to CO_2 (Figure 7D) and also the WGS reaction [18, 24]. This is because of the redox property of ZnO which plays a vital role in catalyst activity for SRE. Moreover, the promotional effects of ZnO might affect the reducibility of NiO at lower temperatures [20, 24,

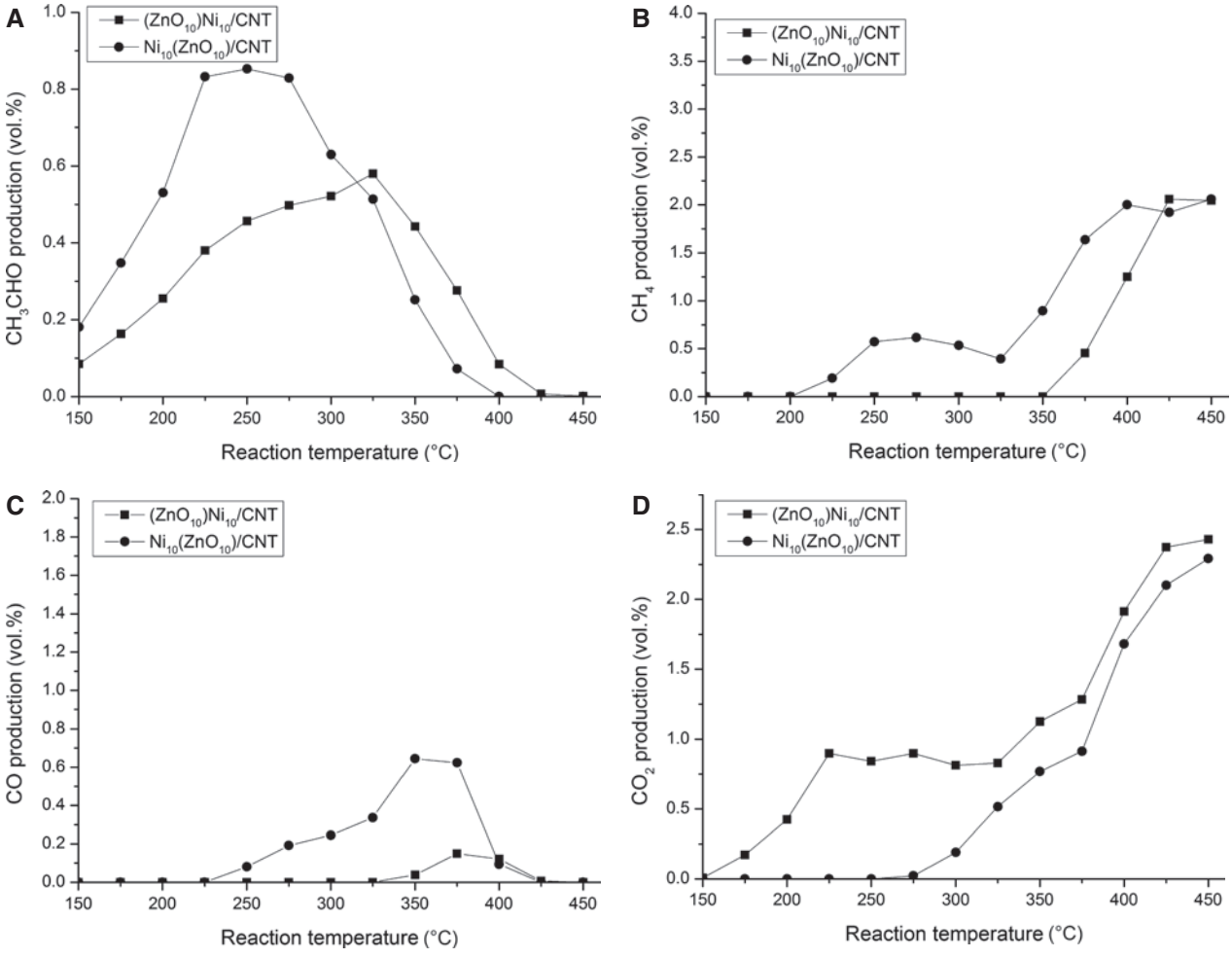

Figure 7: The concentrations of products (A) CH_3CHO, (B) CH_4, (C) CO and (D) CO_2 as a function of reaction temperature over ZnO promoted Ni_{10}/carbon nanotube (CNT) catalysts.

30, 41]. Henceforth, over the ZnO promoted catalysts, the formation of CO is relatively lower compared to all other tested catalysts in SRE. The probable synergistic effects of Ni is to cleave the C-C bond in the ethanol molecule and to promote the segregated ZnO particles which probably reduce the undesirable CO formation. Moreover, the oxygen content in the ZnO promoted catalysts was higher (Table 2) than in the case of the Ni_{10}/CNT catalyst.

The variation in selectivities towards the desired products (i.e. H_2 and CO_2) was observed based on the mode of ZnO addition (Table 4). Over $(ZnO)_{10}Ni_{10}$/CNT catalysts, slightly higher H_2 selectivity was achieved than the $Ni_{10}(ZnO)_{10}$/CNT due to the fact that the ZnO particles are segregated from the Ni counterparts over the CNTs and this might have a positive influence on steam activation by ZnO. In the case of the $Ni_{10}(ZnO)_{10}$/CNT catalyst, Ni might have strong interactions with ZnO, which is indicated by more side reactions, i.e. decomposition and methanation.

Over ZnO promoted catalysts, CH_3CHO might undergo complete reforming and decomposition above 350°C [Eqs. (6) and (7)]. Consequently, the low concentrations of CO and methane are due to the WGS, disproportionation and decomposition reactions. Both the ZnO promoted catalysts exhibit the highest H_2 selectivity of ~60–76% between 150°C and 450°C. The CH_3CHO formation and decomposition reactions are more pronounced over the $Ni_{10}(ZnO)_{10}$/CNT catalysts, and also the WGS activity was lower compared to the $(ZnO)_{10}Ni_{10}$/CNT catalysts. This phenomenon can be seen from the byproducts CH_4 and CO selectivities (Table 4). In the case of the ZnO promoted Ni/CNT catalyst, the bigger ZnO particles on the CNT surface have a greater role in CO reduction to form CO_2 due to the surface oxidation and this facilitates the shift reaction; these phenomena are in good agreement with the previous studies [36, 41, 47]. The byproduct formation rate is very low over $(ZnO)_{10}Ni_{10}$/CNT and thus it is the more ideal catalyst to be developed since it is producing H_2 with very low CO concentration (see Figure 8). By incorporating ZnO to Ni_{10}/CNT, changes in structural and surface properties of the catalyst occur, probably due to the electronic transfer between ZnO and Ni and also with CNT [41].

Table 4: The product selectivity over carbon nanotube (CNT)-based catalysts in steam reforming of ethanol (SRE) reaction as a function of temperature.

T °C	S_{H_2}	S_{CH_3CHO}	S_{CO}	S_{CH_4}	S_{CO_2}
a. $(ZnO_{10})Ni_{10}$/CNT					
300	59.1	16.0	0	0	24.9
350	75.8	6.7	0.6	0	17.0
400	70.8	0.7	1.1	10.8	16.6
450	70.7	0.0	0	13.4	15.9
b. $Ni_{10}(ZnO_{10})$/CNT					
300	66.7	13.1	5.1	11.1	4.0
350	66.3	3.3	8.5	11.8	10.1
400	66.1	0	0.9	18.0	15.1
450	68.9	0	0.1	14.7	16.4

3.5 Deactivation of CNT-based catalysts

The stability was compared between the Ni_{10}/CNT and $(ZnO)_{10}Ni_{10}$/CNT catalysts at 400°C by analyzing ethanol conversion and H_2 production as a function of time-on-stream (TOS) (Table 5). The $(ZnO)_{10}Ni_{10}$/CNT catalyst was selected because of its low CO and CH_4 selectivity at 400°C.

SRE over the Ni_{10}/CNT catalyst achieves ethanol conversion of 95% at the TOS value of 10 min and over the $(ZnO)_{10}Ni_{10}$/CNT catalyst with ~90% conversion. The hydrogen production, i.e. ~9 vol.%, was higher over the ZnO promoted catalyst during the first 90 min. Over the $(ZnO)_{10}Ni_{10}$/CNT catalyst, the ethanol conversion drops from 90% to 78% at the TOS value of 100–120 min and reaches ~70% at 240 min. Further, $(ZnO)_{10}Ni_{10}$/CNT is more stable after 150 min, conversion stabilizes over the period of time, and the decreasing trend is slower compared to the initial drop between 60 min and 75 min. Over the Ni_{10}/CNT catalyst, the ethanol conversion and H_2 production decline significantly from 95% to 52% and 7.8 vol.% to 6.5 vol.%, respectively.

The decreasing trend in the ethanol conversion and hydrogen production was due to the catalyst deactivation. The carbon balance was calculated and it was found that it remains below 100% and indicates carbon deposition during the reaction test. Initially, the carbon balance was close to ~97% at temperatures below 200°C, and the carbon balance decreases with temperature due to the carbon formation via undesirable reactions. Moreover, by EDX analysis, the increment in carbon wt.% (Table 6) in used catalysts was confirmed.

The deactivation of the studied catalysts is attributed to the carbon deposition over the catalyst particles and a significant amount of carbon formation was confirmed by the TEM images (Figure 9). The nature of carbon coating around metal catalysts was as-grown carbon nanofibers/nanotubes and soot. The carbon deposition might occur during the CO disproportionation and decomposition reactions. Further, the catalyst mass before and after the reaction test was measured, and it was found out that the catalyst mass was increased (Table 6). The physical appearance of the used catalysts was different and the formation of more dense and gummy carbon was observed.

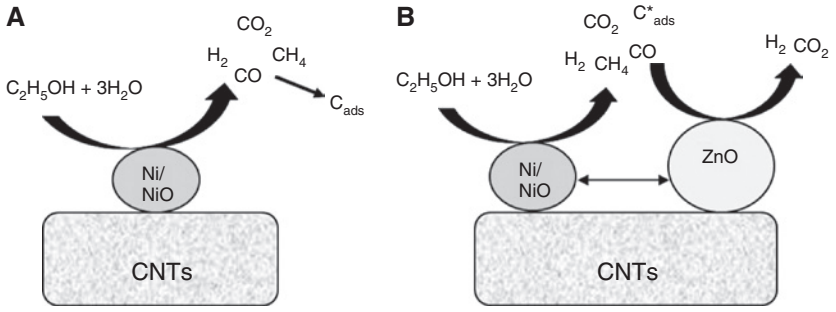

Figure 8: Reaction scheme and possible products and carbon formation during steam reforming of ethanol (SRE) on (A) Ni_{10}/carbon nanotube (CNT) and (B) $(ZnO)_{10}Ni_{10}$/CNT catalysts (carbon amount: C_{ads}>C_{ads}^{*}).

Table 5: Stability of the Ni_{10}/carbon nanotube (CNT) and $(ZnO)_{10}Ni_{10}$/CNT catalysts was analyzed by ethanol conversion and H_2 production (vol.%) at 400°C as a function of time on stream.

Stability test	Ni_{10}/CNT		$(ZnO)_{10}Ni_{10}$/CNT	
Time-on-stream (min)	Conversion (%)	H_2 production (vol. %)	Conversion (%)	H_2 production (vol.%)
10	95	7.8	90	9.1
120	81	6.6	78	8.3
240	52	6.5	70	8.1

Table 6: Textural properties and carbon content of the used Ni_{10}/carbon nanotube (CNT) and $(ZnO)_{10}Ni_{10}$/CNT catalysts.

Catalyst	S_{BET} ($m^2\ g^{-1}$)	Pore volume ($cm^3\ g^{-1}$)	Pore size (nm)	$\Delta m/m_0$ (mg/mg)[a]	Carbon (wt.%)
Ni_{10}CNT	283.9	0.44	6.20	4.6	83.4±3.5
$(ZnO)_{10}Ni_{10}$CNT	271.8	0.40	5.95	2.6	87.7±4.0

[a]m_0, Initial catalyst mass (100 mg); Δm, change in mass (m_{used}–m_{fresh}).

According to [12], with the steam-to-carbon ratio higher than 1.8 there is no coke formation; in this study, the ratio was 1.5 and the carbon/coke deposition is high. The abundant filamentous carbon is observed in addition to different types of carbons formed at the proximity of catalyst particles during the reaction (Figure 9). Significant soot and amorphous carbon formation was found over the Ni_{10}/CNT catalysts (Figure 9A and B). The values presented in Table 6 indicate that minor changes in the textural properties of the used Ni_{10}/CNT and $(ZnO)_{10}Ni_{10}$/CNT catalysts were found after the reaction test for 240 min. The S_{BET} value increased slightly for the Ni_{10}/CNT sample (fresh) from 269.2 $m^2\ g^{-1}$ to 283.9 $m^2\ g^{-1}$ (used); this increment is due to the amorphous carbon deposition over the catalyst surface (Table 6). The amount of adsorbed carbon is relatively high in the case of Ni/CNT (from Figure 8: C_{ads}>C^{*}_{ads}) compared to the ZnO promoted catalyst.

The pore volume and size decreased from 0.66 $cm^3\ g^{-1}$ to 0.44 $cm^3\ g^{-1}$ and 9.4 nm to 6.2 nm, respectively, most probably caused by the soot and carbon nanofibers that covered the nanotube surfaces. The stability of the ZnO promoted catalyst in terms of ethanol conversion and hydrogen production is better compared to Ni_{10}/CNT during the TOS value of 240 min, and the CO and CH_4 concentrations are found to be low. A rapid deactivation was observed over the Ni_{10}/CNT catalyst which might be due to the detected large amounts of encapsulated soot and carbon formation.

4 Conclusions

Ni supported on CNT-based catalysts was studied in the SRE reaction at low temperatures (≤450°C) to produce hydrogen. The surface area of nanotubes was observed to change significantly after the pretreatment steps and it exhibited a mesoporous character. CNTs are promising supports for the ethanol reforming catalysts compared to conventional carbon (activated and graphitic carbon) and alumina supports. Over the CNT-based catalysts, ethanol reforming, CO disproportionation and the WGS reactions

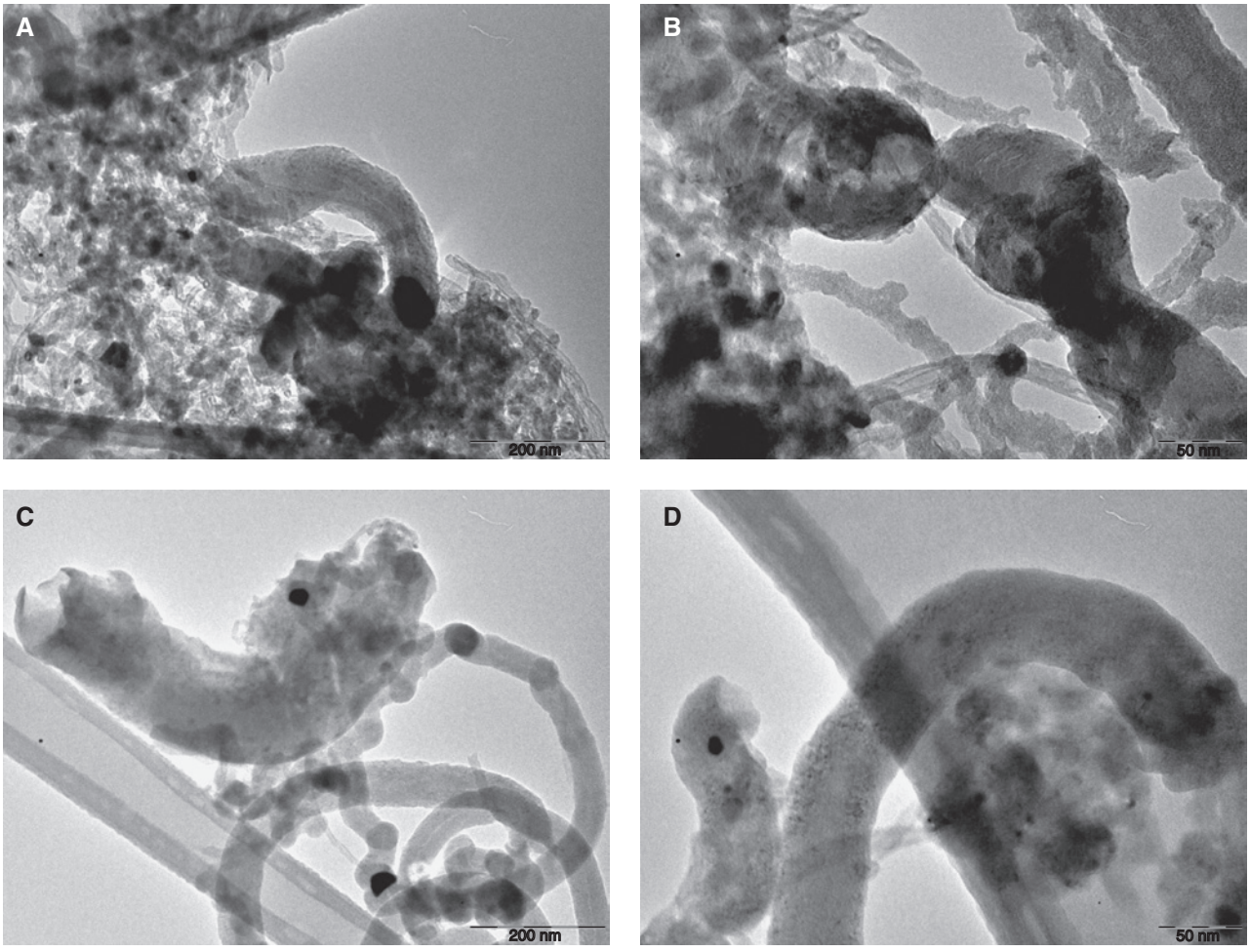

Figure 9: Different types and shapes of carbon formed over carbon nanotube (CNT)-based catalysts during steam reforming of ethanol (SRE). Energy filtered transmission electron micrographs of used catalysts at different magnifications (A, B) Ni_{10}/CNT and (C, D) $(ZnO)_{10}Ni_{10}$/CNT.

are the most probable reactions in the reaction network. For the Al_2O_3-based catalyst, the ethanol decomposition and hydrocarbon (CH_4, C_2H_4) formation are the dominant reactions. The Ni nanoparticle on the CNTs surface displayed narrow distribution with smaller particle sizes (<5 nm). The particle size of Ni was affected by the Pt and ZnO additions due to the successive thermal treatments, i.e. drying, calcination and activation. The ZnO promoted Ni_{10}/CNT catalysts resulted in a superior performance in reforming and the WGS reactions, and reduced the formation of undesirable byproducts such as CH_4 and CO. It was evident that at 350°C, over the $(ZnO)_{10}Ni_{10}$/CNT catalyst complete ethanol conversion with ~76% H_2 and less than 1% CO selectivity were achieved. Moreover, the $(ZnO)_{10}Ni_{10}$/CNT catalyst is more stable compared to Ni_{10}/CNT for the period of 240 min according to the stability test. The deactivation rate of the promoted catalysts is slower than that of the Ni_{10}/CNT catalyst. Future work is needed to improve the stability of the catalysts and to understand the carbon deposition phenomenon and reactions at low temperatures.

Acknowledgments: The financial support from the Finnish Funding Agency for Innovation (Tekes), and from the Academy of Finland (project no: 128783) are acknowledged. Ms. A.-R. Rautio is grateful for the position received from GETA. The authors want to acknowledge Mr. J. Penttinen for surface area measurements.

References

[1] Holladay JD, Hu J, King DL, Wang Y. *Catal. Today* 2009, 139, 244–260.
[2] Pudukudy M, Yaakob Z, Mohammad M, Narayanan B, Sopian K. *Renew. Sustain. Energy Rev.* 2014, 30, 743–757.
[3] Kleijn R, Van der Voet E. *Renew. Sustain. Energy Rev.* 2010, 14, 2784–2795.

[4] Andrews J, Shabani B. *Int. J. Hydrogen Energy* 2012, 37, 1184–1203.
[5] Navarro RM, Pena MA, Fierro JL. *Chem. Rev.* 2007, 107, 3952–3991.
[6] Mattos LV, Jacobs G, Davis BH, Noronha FB. *Chem.* Rev. 2012, 112, 4094–4123.
[7] Liguras DK, Kondarides DI, Verykios XE. *Appl. Catal. B* 2003, 43, 345–354.
[8] Ni M, Leung DYC, Leung MKH. *Int. J. Hydrogen Energy* 2007, 32, 2238–2247.
[9] Roh H-S, Wang Y, King DL, Platon A, Chin Y-H. *Catal. Lett.* 2006, 108, 1–2.
[10] Seelam PK, Huuhtanen M, Sápi A, Kordás K, Szabó M, Turpeinen E, Keiski RL. *Int. J. Hydrogen Energy* 2010, 35, 12588–12595.
[11] Morgenstern DA, Fornango JP. *Energy Fuels* 2005, 19, 1708–1716.
[12] Li J, Yu H, Yang G, Peng F, Xie D, Wang H, Yang J. *Energy Fuels* 2011, 25, 2643–2650.
[13] Panagiotopoulou P, Verykios XE. *Int. J. Hydrogen Energy* 2012, 37, 16333–16345.
[14] Chen L, Choong CKS, Zhong Z, Huang L, Ang TP, Hong L, Lin J. *J. Catal.* 2010, 276, 197–200.
[15] Liberatori JWC, Ribeiro RU, Zanchet D, Noronha FB, Bueno JMC. *Appl. Catal. A.* 2007, 327, 197–204.
[16] Zhang H, Yang D, Li B, Qian Z, Ma J. *Int. J. Energy Res*. 2014, 38, 277–284.
[17] Lee JS, Han GB, Kang M. *Energy* 2012, 44, 248–256.
[18] Llorca J, Piscina PR, Dalmon JA, Sales J, Homs N. *Appl. Catal. B.* 2003, 43, 355–369.
[19] Sun J, Qiu XP, Wu F, Zhu WT. *Int J Hydrogen Energy* 2005, 30, 437–445.
[20] Llorca J, Piscina PR, Sales J, Homs N. *Chem. Commun.* 2001, 641–642.
[21] Yang Y, Ma J, Wu F. *Int. J. Hydrogen Energy* 2006, 31, 877–882.
[22] Homs N, Llorca J, Piscina PR. *Catal.* Today 2006, 116, 361–366.
[23] Llorca J, Homs N, Sales J, Piscina PR. *J. Catal.* 2002, 209, 306–317.
[24] Davidson S, Sun J, Wang Y. *Top. Catal.* 2013, 56, 1651–1659.
[25] Sápi A, Rémiás R, Kónya Z, Kukovecz A, Kordás K, Kiricsi I. *React. Kinet. Catal. Lett.* 2009, 96, 379–389.
[26] Halonen N, Rautio A, Leino AR, Kyllönen T, Tóth G, Lappalainen J, Kordás K, Huuhtanen M, Keiski RL, Sápi A, Szabó M, Kukovecz A, Kónya Z, Kiricsi I, Ajayan PM, Vajtai R. *ACS Nano* 2010, 4, 2003–2008.
[27] Chen Z, Guan Z, Li M, Yang Q, Li C. *Angew. Chem., Int. Ed.* 2011, 50, 4913–4917.
[28] Leino AR, Mohl M, Kukkola J, Mäki.-Arvela P, Kokkonen T, Shchukarev A, Kordas K. *Carbon* 2013, 57, 99–107.
[29] Hou T, Yuan L, Ye T, Gong L, Tu J, Yamamoto M, Torimoto Y, Li Q. *Int. J. Hydrogen Energy* 2009, 22, 9095–9107.
[30] Yang HM, Liao PH. *Appl. Catal. A.* 2007, 317, 226–233.
[31] López E, Kim J, Shanmugharaj AM, Ryu SH. *J. Mater. Sci.* 2012, 47, 2985–2994.
[32] Barthos R, Széchenyi A, Solymosi F. *Catal. Lett.* 2008, 120, 161–165.
[33] Soyal-Baltacıloglu F, Aksoylu AE, Önsan ZI. *Catal. Today* 2008, 138, 183–186.
[34] Furtado AC, Alonso CG, Cantão MP, Fernandes-Machado NRC. *Int. J. Hydrogen Energy* 2009, 34, 7189–7196.
[35] Profeti LPR, Ticianelli EA, Assaf EM. *Int. J. Hydrogen Energy* 2009, 34, 5049–5060.
[36] Profeti LPR, Dias JAC, Assaf JM, Assaf EM. *J. Power Sources* 2009, 190, 525–533.
[37] Azadi P, Farnood R, Meier E. *J. Phys. Chem. A* 2010, 114, 3962–3968.
[38] Ivanova E, Karsheva M. *J. Univ. Chem. Technol. Metall.* 2007, 42, 391–398.
[39] Arishtirova K, Pawelec B, Nikolov RN, Fierro JLG, Damyanova S. *Kinet. Catal. Lett.* 2007, 91, 241–248.
[40] Pan X, Bao X. *Chem. Commun.* 2008, 47, 6271–6281.
[41] Buitrago-Sierra R, Ruiz-Martínez J, Serrano-Ruiz JC, Rodríguez-Reinoso F, Sepúlveda-Escribano A. *J. Colloid Interface Sci.* 2012, 383, 148–154.
[42] Elizabeth GM, Pusel JM, Stagg-Williams SM, Faraji S. *J. CO2 Utilization* 2014, 6, 40–44.
[43] Kordás K, Mustonen T, Tóth G, Jantunen H, Lajunen M, Soldano C, Talapatra S, Kar S, Vajtai R, Pulickel AM. *Small* 2006, 2, 1021–1025.
[44] Seelam PK. D.Sc. (Tech.) thesis: Hydrogen production by steam reforming of bio-alcohols: the use of conventional and membrane-assisted catalytic reactors, Copy right permission from University Oulu, ACTA series C473: ISBN 978-952-62-0277-8, 4 Dec 2013.
[45] de Souza VP, Costa D, dos Santos D, Sato AG, Bueno JMC. *Int. J. Hydrogen Energy* 2012, 37, 9985–9993.
[46] Jiang HJ, Tzou MS, Sachtler WHM. *Catal. Lett.* 1988, 1, 99–107.
[47] Chen MN, Zhang DY, Thompson LT, Ma ZF. *Int. J. Hydrogen Energy* 2011, 36, 7516–7522.

Supplemental Material: The online version of this article (DOI: 10.1515/gps-2015-0014) offers supplementary material, available to authorized users.

Bionotes

Prem Kumar Seelam

Prem Kumar Seelam obtained his DSc (Tech) in Process Engineering at the University of Oulu (2013) and MSc in Chemical Engineering at the Abo Akademi University (2007). He is currently working as a postdoctoral researcher in the Environmental and Chemical Engineering research group, University of Oulu, Finland. His research work is focused on heterogeneous catalysis and reaction engineering. His work emphasizes catalysts design and development for hydrogen production, CO_2 utilization reactions and also membrane assisted reactors for clean energy and environmental technologies. He worked in many international collaborative research projects and networking in the EU, Cost Action, Indo-EU, and FP7 Marie Curie Actions.

Anne-Riikka Rautio

Anne-Riikka Rautio (née Leino) graduated with an MSc in Organic Chemistry (2010, University of Oulu, Finland). In 2008, she joined the Microelectronics and Materials Physics Laboratories as a research assistant. Since 2010, she has been pursuing studies towards her PhD with topics relating to the formation and agglomeration of nanoparticles over nanostructured surfaces. In 2011, she received a 4 year position in the Graduate School in Electronics, Telecommunications and Automation, GETA.

Mika Huuhtanen

Mika Huuhtanen is a Docent in Chemical Process Engineering, especially in applied heterogeneous catalysis at the University of Oulu, Finland. He defended his doctoral thesis in 2006, continued as a postdoctoral researcher, and has been a coordinator and a responsible leader in projects funded by the Academy of Finland and Tekes. In addition, he is currently a steering group member in two national Centre for Science, Technology and Innovation (CSTI) programs. Since 2011, he held a university lecturer position. He is an author of approximately 50 scientific papers published in refereed international journals and five book chapters, and has given more than 80 invited, oral and poster presentations in conferences and seminars. His expertise areas are heterogeneous catalysis, pollution prevention and mitigation, energy production and surface characterization techniques.

Krisztian Kordas

Krisztian Kordas studied for an MSc in Physics and Chemistry (1998, University Szeged, Hungary), is a DSc (Tech) in Microelectronics and Docent of Nanotechnology (2002 and 2005, University Oulu, Finland). He has held a position as a research professor at the Department of Electrical Engineering, University of Oulu since 2013. His research is focused on the synthesis and application of nanostructured materials and their assemblies implemented in electrical and sensing devices as well as in (photo) catalytic systems.
Dr Kordas has authored 120+ peer-reviewed scientific papers and book chapters in materials science and technology.

Riitta L. Keiski

Riitta L. Keiski [DSc (Tech) in 1991] is a Professor in the Environmental and Chemical Engineering Research Group (since 2001) and the Dean of the Faculty of Technology at the University of Oulu. She was the vice rector of the University of Oulu from 2006 to 2009 and a Member of the Board of the Academy of Finland from 2001 to 2006 and 2014 onwards. She is the Head of the Environmental and Chemical Engineering Research Group and the Director of the Advanced Materials doctoral program. She is a Docent in Chemical Process Engineering, especially in Heterogeneous Catalysis and Environmental Engineering. In education and research, Professor Keiski's fields are process and environmental catalysis, air and water pollution control, reactor and separation unit and sustainability assessment tools design, and research ethics. Carbon dioxide utilization, environmental catalysis, biofuels production and membrane and adsorption materials studies have been the key research areas for more than a decade.